Strong plasma screening in thermonuclear reactions: Electron drop model

P. A. Kravchuk[1] and D. G. Yakovlev[2]

[1]*St. Petersburg State Polytechnical University, Politekhnicheskaya 29, St. Petersburg 195251, Russia*
[2]*Ioffe Physical Technical Institute, Politekhnicheskaya 26, St. Petersburg 194021, Russia*

We analyze enhancement of thermonuclear fusion reactions due to strong plasma screening in dense matter using a simple electron drop model. In the model we assume fusion in a potential that is screened by an effective electron cloud around colliding nuclei (extended Salpeter ion-sphere model). We calculate the mean-field screened Coulomb potentials for atomic nuclei with equal and nonequal charges, appropriate astrophysical *S* factors, and enhancement factors of reaction rates. As a byproduct, we study the analytic behavior of the screening potential at small separations between the reactants. In this model, astrophysical *S* factors depend not only on nuclear physics but on plasma screening as well. The enhancement factors are in good agreement with calculations by other methods. This allows us to formulate a combined, pure analytic model of strong plasma screening in thermonuclear reactions. The results can be useful for simulating nuclear burning in white dwarfs and neutron stars.

PACS number(s): 26.60.Gj, 97.20.Rp

I. INTRODUCTION

It is well known that nuclear reactions in compact stars, which contain matter of high density, can be strongly modified by plasma physics effects (e.g., Ref. [1]). Under compact stars we mean white dwarfs and neutron stars [2]. Central densities of massive white dwarfs can be as high as 10^{10} g cm^{-3}. Carbon and oxygen burning in the cores of white dwarfs is thought to trigger type Ia supernova explosions (e.g., Refs. [3,4]). Neutron stars contain outer and inner crusts, where atomic nuclei are available and can participate in various reactions which result in steady-state and explosive burning and nucleosynthesis [5–7]. For instance, we can mention helium or carbon burning, leading to type I x-ray bursts or superbursts; these reactions occur at densities $\lesssim 10^{10}$ g cm^{-3}.

The plasma physics effects modify the reactions at sufficiently high densities and not very high temperatures when the plasma of atomic nuclei becomes strongly nonideal due to strong Coulomb coupling. At these conditions, the well-known classical thermonuclear burning regime [8] is no longer valid. With increasing density and/or decreasing temperature, one has a sequence of four other nuclear burning regimes [1]: thermonuclear burning with strong plasma screening, intermediate thermo-pycnonuclear burning, thermally enhanced pycnonuclear burning, and temperature-independent pycnonuclear burning.

In this paper we address the thermonuclear burning with strong plasma screening, which is realized in a wide range of temperatures and densities of matter and is important for applications in compact stars. In this regime, the plasma of atomic nuclei (ions) is strongly coupled but mostly classical (i.e., quantum effects on the motion of ions are weak). The plasma effects are well known to enhance thermonuclear reaction rates and are conveniently described by the enhancement factor

$$f = R/R_0 \quad (f \geqslant 1), \qquad (1)$$

where R is the actual rate and R_0 is the rate calculated by neglecting plasma screening. Unless the contrary is indicated,

subscript 0 will mark quantities calculated with the screening neglected. The factor f will be the basic quantity of our interest. It has been calculated using different techniques and approximations in a number of publications cited in Sec. IV, starting from the seminal paper by Salpeter [9].

Our aim here is to consider a simple model for strong plasma screening in thermonuclear reactions. In Sec. II we outline physical conditions in dense stellar matter. In Sec. III we formulate the model. Then we consider the mean plasma screening potentials (Sec. IV), the basic Salpeter model for plasma screening in thermonuclear reactions (Sec. V), as well as astrophysical *S* factors (Sec. VI) and enhancement factors (Sec. VII) for our model. In Sec. VIII we discuss our main results and propose a combined analytic model for strong plasma screening in the thermonuclear regime; we conclude in Sec. IX. Some technical details are presented in the Appendices.

II. PLASMA PARAMETERS

Atomic nuclei in dense stellar matter are fully ionized by enormous electron pressure, and the electrons are so energetic that they constitute almost a rigid background of negative charge in which the ions move. Generally, we have a multicomponent ion mixture because we study nuclear fusion reactions involving equal or different nuclei, and the reaction products (daughter nuclei) are also present there. We consider a mixture of ion species $j = 1, 2, \ldots$, with atomic numbers A_j and charge numbers Z_j. Let n_j be the number density of ions j. The total number density of ions is $n = \sum_j n_j$; the electron number density is $n_e = \sum_j Z_j n_j$.

It is convenient to introduce the Coulomb coupling parameter Γ_j for ions j (e.g., Ref. [10]), given as

$$\Gamma_j = \frac{Z_j^2 e^2}{a_j k_B T} = \frac{Z_j^{5/3} e^2}{a_e k_B T},$$

$$a_e = \left(\frac{3}{4\pi n_e}\right)^{1/3}, \quad a_j = Z_j^{1/3} a_e, \qquad (2)$$

where T is the temperature, k_B is the Boltzmann constant, a_e is the electron-sphere radius, and a_j is the ion-sphere radius (for a sphere around a given ion, where the electron charge compensates the ion charge). Therefore, Γ_j is the ratio of the typical electrostatic energy of the ion to the thermal energy. If $\Gamma_j \ll 1$ then the ions constitute an almost ideal Boltzmann gas, while for $\Gamma_j \gtrsim 1$ they are strongly coupled by Coulomb forces (constituting either a Coulomb liquid or solid).

The strongly coupled plasma is accurately described as an ensemble of closely packed ion spheres. The Coulomb energy of the ion sphere (including the electrostatic energy of the electron cloud and the energy of electron-ion interaction) is

$$W(Z) = -\frac{9}{10}\frac{e^2 Z^2}{a_j} = -\frac{9}{10}\frac{e^2 Z^{5/3}}{a_e}. \quad (3)$$

Let us consider a fusion reaction $(A_1, Z_1) + (A_2, Z_2) \to (A_c, Z_c)$, with $A_c = A_1 + A_2$ and $Z_c = Z_1 + Z_2$ (where subscript c refers to a compound nucleus), and introduce the parameters

$$a_c = a_e Z_c^{1/3}, \quad a_{12} = \frac{a_1 + a_2}{2}, \quad E_{12} = \frac{Z_1 Z_2 e^2}{a_{12}}, \quad (4)$$

$$\Gamma_{12} = \frac{E_{12}}{k_B T}, \quad \tau = \left(\frac{27\pi^2 \mu Z_1^2 Z_2^2 e^4}{2 k_B T \hbar^2}\right)^{1/3}, \quad \zeta = \frac{3\Gamma_{12}}{\tau}. \quad (5)$$

Here, $\mu = m_1 m_2/(m_1 + m_2)$ is the reduced mass of the reactants, E_{12} is a convenient unit of their electrostatic energy, τ is the basic parameter of thermonuclear reactions, and ζ measures the importance of quantum effects in ion motion for thermonuclear reactions. In stellar matter one usually has $\tau \gg 1$; $\exp(-\tau)$ determines the probability of quantum tunneling through the Coulomb barrier with plasma screening neglected. Let E be the center-of-mass energy of the nuclei. Then the typical (Gamow-peak) energy which contributes to the thermonuclear reaction with plasma screening neglected is $E_{p0} = k_B T \tau/3$. Introducing a convenient dimensionless center-of-mass energy ϵ we obtain

$$\epsilon = E/E_{12}, \quad \epsilon_{p0} = E_{p0}/E_{12} = 1/\zeta. \quad (6)$$

We consider thermonuclear burning with strong plasma screening in which both reacting ions are strongly coupled ($\Gamma_1 \gg 1$ and $\Gamma_2 \gg 1$; liquid or solid) but quantum effects are relatively weak ($\zeta \lesssim 1$). For a one-component ion plasma ($Z_1 = Z_2$, $A_1 = A_2$) this would correspond to the range of temperatures $0.34 T_p \lesssim T \ll T_l$, where T_l is the temperature of strong coupling ($\Gamma \simeq 1$), and $T_p = \hbar\omega_p/k_B$ is the ion plasma temperature determined by the ion plasma frequency $\omega_p = \sqrt{4\pi Z^2 e^2 n/m}$ (close to the Debye temperature of the one-component Coulomb crystal). The temperature range under discussion spans typically over 1–2 orders of magnitude.

For example, Fig. 1 shows the temperature-density diagram for a ^{12}C plasma. The upper thick line is the temperature T_l of strong Coulomb coupling. Above this line (weakly dashed region in the upper left corner) carbon is burning in the classical thermonuclear regime where plasma screening is weak. The lower thick line is $T = 0.34 T_p$, below which
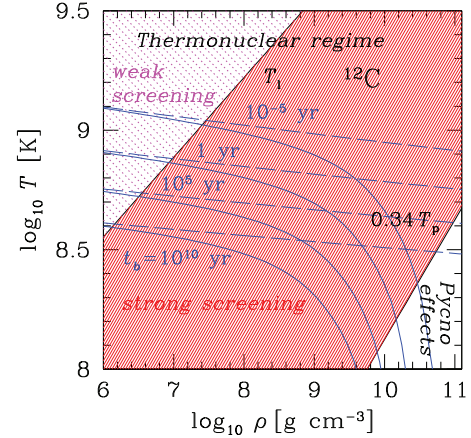

FIG. 1. (Color online) Temperature-density diagram for a ^{12}C plasma. Shaded is the temperature-density domain for ^{12}C matter where carbon burns in the thermonuclear regime. The domain of dense shading refers to the thermonuclear regime with strong screening. Its upper boundary is determined by the temperature T_l at which ions become strongly coupled, while the lower boundary is taken to be $0.34 T_p$. The four thin solid lines are those at which characteristic carbon burning time is $t_b = 10^{10}$, 10^5, 1, and 10^{-5} years; the four thin dashed lines are the same but with plasma physics effects neglected (see text for details).

(in the nondashed region) pycnonuclear effects in carbon burning become important. The densely shaded area is the domain where the burning is thermonuclear with strong plasma screening—the main subject of our study. To illustrate the efficiency of carbon burning, four thin solid curves show the lines along which the carbon burning time, defined as $t_b = n/R$, is constant (from bottom to top), $t_b = 10^{10}$, 10^5, 1, and 10^{-5} years. The reaction rate R is calculated using the formalism of Ref. [11]. The plasma physics effects [of strong screening and pycnonuclear ("pycno") burning] are included and cause the bend of the t_b curves at high densities and low temperatures. Carbon burning is extremely slow below the $t_b = 10^{10}$ year line and fast above the $t_b = 10^{-5}$ year line. The four thin dashed lines are the same as the thin solid lines but do not include plasma physics effects. One can see that at high densities and not too high temperatures these effects are most important. More information on the efficiency of carbon burning in the different regimes can be found, for instance, in Ref. [11].

III. MODEL

Let us formulate our model for thermonuclear reactions with strong plasma screening.

At the first stage (Sec. IV) we introduce the Coulomb potential $U_C(r)$ for pointlike colliding atomic nuclei in the standard form

$$U_C(r) = \frac{Z_1 Z_2 e^2}{r} - H(r), \quad (7)$$

where $H(r)$ is the mean-field plasma screening potential to be determined. We will calculate $H(r)$ in the spirit of the ion-sphere model suggested by Salpeter [9]. We assume that $H(r)$
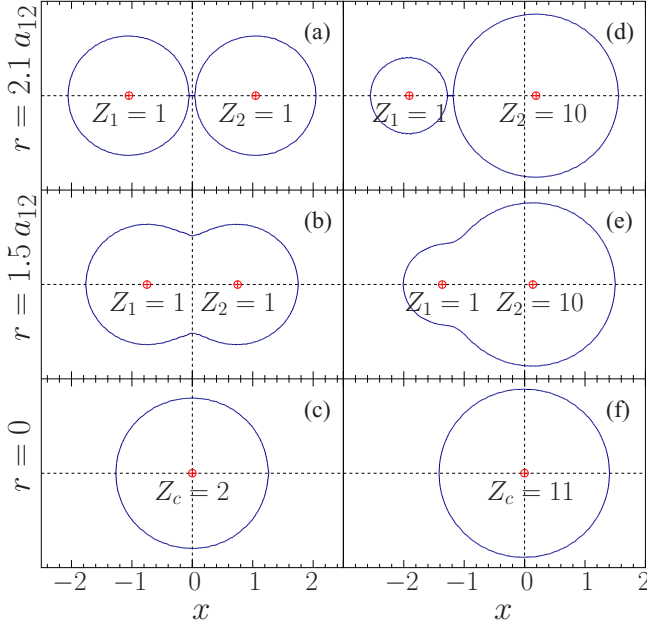
FIG. 2. (Color online) Simulated shapes of the electron drops around two colliding nuclei for $Z_2 = Z_1$ at inter-ion distances of (a) 2.1 a_{12}, (b) 1.5 a_{12}, and (c) 0 and for $Z_2 = 10 Z_1$ at inter-ion distances of (d) 2.1 a_{12}, (e) 1.5 a_{12}, and (f) 0.

is produced by an electron cloud around the reactants. Such systems of ions surrounded by electron clouds in dense matter are sometimes called Onsager molecules (e.g., Ref. [12], and references therein). We assume rigid electron charge density, and we view the electron cloud as an incompressible uniformly charged liquid drop. The electron drop has constant volume; its charge fully compensates for the electric charge of the reactants. However, it has variable shape, which minimizes the Coulomb energy of the system (of the electron drop and the two reactants). It acts as a Wigner-Seitz cell in which the ions tunnel. In Fig. 2 we show the calculated electron drop shapes for several inter-ion distances and charge ratios.

This model for $H(r)$ is expected to be adequate in the regime of strong Coulomb coupling. For weak coupling, the plasma screening would be too weak to be described by an electron drop with a sharp boundary; anyway, it would have no strong effect on thermonuclear burning rates—see, e.g., Ref. [9]. Our model, like the Salpeter model [9], is so simple that it does not distinguish the cases of strong coupling in Coulomb liquid and solid (since the effects of background ions are tacitly described by the electron drop).

At the next stage (Sec. VI) we calculate the astrophysical S factors for thermonuclear reactions by adding the screening potential to the total potential in which the nuclei fuse. In this way we include the screening effect into the S factor, so that the modified S factor becomes determined not only by nuclear interactions but also by the parameters of dense matter.

Finally, in Sec. VII we calculate the reaction rates R for thermonuclear reactions with the modified astrophysical S factors in a standard way, assuming a Maxwellian velocity distribution of the reactants. With these rates we determine the plasma screening enhancement factors f from Eq. (1).

Our model is well defined and easily realized. It will be compared with other available models for thermonuclear reactions with strong plasma screening.

IV. PLASMA SCREENING POTENTIAL

Let us calculate the screening potential $H(r)$ in the electron drop model. At large separations we have

$$H(r) = \frac{Z_1 Z_2 e^2}{r}, \quad U_C(r) \equiv 0 \quad \text{at} \quad r \geqslant (a_1 + a_2). \quad (8)$$

In this case each reacting ion is surrounded by its own ion sphere of radius a_1 or a_2. The electrons within these ion spheres fully compensate for the ion charges, making the ion spheres electrically neutral (and, hence, noninteracting). The electrostatic energy of these two spheres is

$$W_{12} = W(Z_1) + W(Z_2) = -\frac{0.9 e^2}{a_e} \left(Z_1^{5/3} + Z_2^{5/3} \right). \quad (9)$$

At smaller separations, $r < (a_1 + a_2)$, the two ion spheres merge, forming one common electron drop, so that $U_C(r)$ becomes finite.

It is convenient to write

$$H(r) = E_{12} h(x), \quad x = \frac{r}{a_{12}}, \quad (10)$$

where $h(x)$ is a dimensionless function of a dimensionless radial coordinate x. The critical separation $r = (a_1 + a_2)$ corresponds to $x = 2$, and at $x \geqslant 2$ we have $h(x) = 1/x$. At $x \ll 2$ the function $h(x)$ is expandable as

$$h(x) = b_0 + b_2 x^2 + b_4 x^4 + \cdots. \quad (11)$$

The expansion coefficients $b_0, b_2, b_4, \ldots$ appear to depend on only one parameter:

$$z = Z_2/Z_1, \quad (12)$$

with $z = 1$ for equal charges $Z_1 = Z_2$, and $z \neq 1$ for $Z_1 \neq Z_2$. The normalized potential $h(x)$ is symmetric with respect to $z \to 1/z$, so that it is sufficient to consider the case of $z \geqslant 1$.

The first expansion coefficients are (see Appendix A)

$$b_0 = \frac{0.9}{2z} [(1+z)^{5/3} - 1 - z^{5/3}](1 + z^{1/3}), \quad (13)$$

$$b_2 = -\frac{1}{16} \frac{(1 + z^{1/3})^3}{1+z}, \quad (14)$$

$$b_4 = \frac{z}{64} \frac{(1 + z^{1/3})^5}{(1+z)^{11/3}}. \quad (15)$$

The expression for b_0 was obtained by Salpeter [9]; b_2 for $z = 1$ was derived by Jancovici [13] and was generalized for $z \neq 1$ by Ogata et al. [14]. The expression for b_4 seems to be original. For $z = 1$ we have $b_0 \approx 1.0573$, $b_2 = -0.25$, and $b_4 \approx 0.0394$.

Although Eqs. (13)–(15) are derived within the electron drop model, they accurately describe the real potential $h(r)$. The applicability of Eq. (13) has been confirmed by numerous Monte Carlo (MC) simulations. The coefficient b_2 is basically the contribution from the electron background. As shown by

Jancovici [13], neighboring ions do not contribute to this order, making Eq. (14) quite robust.

The leading term in the expansion (11) gives [9]

$$H(0) = H_0 = E_{12} b_0 = W(Z_c) - W_{12}, \qquad (16)$$

which is the difference of electrostatic ion-sphere energies for the compound nucleus and the two reacting nuclei.

It is important that $H(0)$ be accurately determined from numerous MC simulations of strongly coupled multicomponent ion mixtures. These simulations are superior to the electron drop model. The results indicate that strongly coupled mixtures obey a linear mixing rule (see, e.g., Ref. [10]), according to which

$$H(0)_{\mathrm{MC}}/k_B T = f_C(\Gamma_1) + f_C(\Gamma_2) - f_C(\Gamma_c), \qquad (17)$$

where $f_C(\Gamma)$ is the Coulomb free energy per ion in units of $k_B T$ in a strongly coupled one-component plasma. Then the MC value of b_0 is

$$b_0^{\mathrm{MC}} = [f_C(\Gamma_1) + f_C(\Gamma_2) - f_C(\Gamma_c)]/\Gamma_{12}. \qquad (18)$$

The function $f_C(\Gamma)$ has been accurately calculated by various methods and fitted by analytic expressions. For instance, one can use a fit from Ref. [15] (for a one-component ion gas and liquid),

$$
\begin{aligned}
f_C(\Gamma) = A_1 & \left[\sqrt{\Gamma(A_2 + \Gamma)} - A_2 \ln \left(\sqrt{\frac{\Gamma}{A_2}} + \sqrt{1 + \frac{\Gamma}{A_2}} \right) \right] \\
& + 2 A_3 (\sqrt{\Gamma} - \arctan \sqrt{\Gamma}) \\
& + B_1 \left[\Gamma - B_2 \ln \left(1 + \frac{\Gamma}{B_2} \right) \right] \\
& + \frac{B_3}{2} \ln \left(1 + \frac{\Gamma^2}{B_4} \right),
\end{aligned}
\qquad (19)
$$

where $A_1 = -0.907$, $A_2 = 0.62954$, $B_1 = 0.00456$, $B_2 = 211.6$, $B_3 = -0.0001$, $B_4 = 0.00462$, and $A_3 = -\sqrt{3}/2 - A_1/\sqrt{A_2} = 0.2771$.

Now let us return to the electron drop model. In addition to the analytic small-x expansion (11), we have calculated $h(x)$ numerically. The numerical algorithm is as follows. First, two pointlike ions are set at a given separation, surrounded by an electron liquid drop of compensating charge symmetrical with respect to the inter-ion axis. Then several thousand passes are run. At each pass we calculate the electrostatic potential and optimize the drop shape by rearranging small portions of the electron liquid.

Calculations have been done for the values of z ranging from 1 to 10 with a step size of 0.5. Numerical errors have been estimated by comparing with the exact analytic results at $r = 0$ and $r = a_1 + a_2$. We have also compared the numerical results at low r with the analytic expansion (11) [including the three terms, Eqs. (13)–(15)]. The estimated numerical errors are $\lesssim 0.2\%$.

For convenience of applications we have approximated the numerical data ($0 \leqslant x \leqslant 2$) by the analytic expression

$$h(x) = \left[\left(1 - \frac{x^2}{4} \right)^2 (p_0 + p_2 x^2 + p_4 x^4) + x^2 \right]^{-1/2}, \quad (20)$$

with

$$
\begin{aligned}
p_0 &= \frac{1}{b_0^2}, \\
p_2 &= \frac{p_0}{2} - \frac{2 b_2}{b_0^3} - 1, \\
p_4 &= \frac{3 b_2^2}{b_0^4} - \frac{2 b_4}{b_0^3} - \frac{p_0}{16} + \frac{p_2}{2},
\end{aligned}
\qquad (21)
$$

with b_0, b_2, and b_4 being given by Eqs. (13)–(15). For $z = 1$ we have $p_0 = 0.8945$, $p_2 = -0.1297$, and $p_4 = -0.0374$. The analytic fit is constructed in such a way that it correctly reproduces the small-x expansion (11) (including three terms); it also reproduces the correct value $h(2) = 1/2$, smoothly matching $1/x$ at $x = 2$. The formal fit errors are less than 0.2% (comparable with the numerical errors).

We have also considered some other $h(x)$ approximations. In particular, we have tried a polynomial expansion (11) in x^2 keeping five terms. The coefficients b_0, b_2, and b_4 have been set equal to their exact analytic values, while b_6 and b_8 have been chosen in such a way to match smoothly $h(x) = 1/x$ at $x \geqslant 2$. This approximation is as accurate as (20); the expressions for b_6 and b_8 are cumbersome (and not presented here).

The screening potential has been studied and approximated by a number of authors (e.g. [14,16–19], and references therein). Itoh *et al.* [18] used a not very accurate approximation matching the $1/x$ behavior with $h(0)$ by linear functions. Ogata *et al.* [14] (OII91) determined the potential from MC simulations. Their $h(0)$ was improved later in MC calculations by Caillol and Gilles [19], as well as by DeWitt and Slattery [20] and Caillol [21]. Itoh *et al.* [17] (ITWN03) used $h(0)$ obtained by Jancovici [13]; relying on the expression (14) for b_2 they matched the linear behavior of the potential near $x = 2$. Chugunov, DeWitt, and Yakovlev [16,22] (CDW09) constructed the screening potential from the results of Ref. [15] and from their own MC data.

In Fig. 3 we compare our electron drop results with those obtained previously (for a one-component strongly coupled plasma of ions). At $x > 1$ all curves are in good agreement but slightly differ from our electron drop fit. At smaller x the OII91 data deviate from others (due to poor MC statistics in OII91 at small x). Our results differ due to simplicity of the electron drop model. The combined curve, obtained from our fit (20) with b_0 given by Eq. (18) instead of the electron drop value, Eq. (13), closely reproduces the data of CDW09 and ITWN03. The combined approximation is also discussed in Sec. VIII. From the insert (b) we see that MC-based results (CDW09 and OII91) deviate from others. While these results for the mean-field potential are superior to other fits, this discrepancy only occurs at distances $x \gtrsim 1.2$, whereas for the discussed case of $\zeta \lesssim 1$ all turning points at Gamow-peak energies have $x < 1$. Note that for $\zeta \gtrsim 1$ our consideration of thermonuclear burning becomes questionable (Secs. V and VI).

V. SALPETER'S MODEL

Before we focus on the full electron drop model we outline a simpler (basic) model for plasma screening in thermonuclear reactions. We will do it in the spirit of Salpeter's model [9]
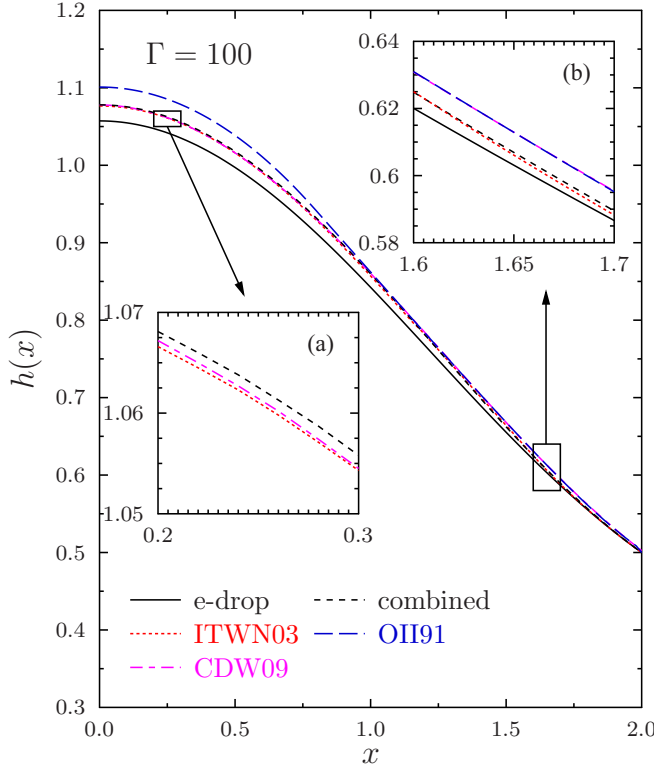
FIG. 3. (Color online) Screening potential $h(x)$ vs x at $z = 1$. Solid lines show our electron drop (e-drop) fit; dot-dashed lines are the fits by Chugunov and DeWitt [16]; long-dashed lines are from Ogata *et al.* [14], dotted lines are from Itoh *et al.* [17]; short-dashed lines represents the combined fit. Inserts are expanded regions showing the behavior of $h(x)$ at $x \simeq 0.25$ (a) and at larger $x \simeq 1.65$ (b). See text for details.

of ion spheres and call it Salpeter's model. The quantities calculated within this model will be labeled by the index S. In this model, the screening potential is replaced by the constant potential H_0, which is given by Eq. (16) and corresponds to the leading term $h(x) = b_0$ in the expansion (11). Then the Coulomb energy (7) becomes

$$U_C^{(S)}(r) = \frac{Z_1 Z_2 e^2}{r} - H_0. \qquad (22)$$

This constant (r-independent) screening potential H_0 is determined by the density of the matter. For a reaction between identical nuclei, $H_0 = 1.0573 Z^2 e^2 / a_1$. The respective plasma screening does not change the shape of $U_C(r)$ but simply lowers the pure Coulomb potential $Z_1 Z_2 e^2 / r$ by H_0, which enhances naturally the nuclear fusion rate.

The well-known expression for a thermonuclear reaction rate adopted here is

$$R = \chi \, n_1 n_2 I, \quad I = \int_0^\infty dE \, S(E) \exp\left(-2\pi\eta - \frac{E}{k_B T}\right), \qquad (23)$$

where χ is a symmetry factor ($\chi = \frac{1}{2}$ for a reaction with identical nuclei, and $\chi = 1$ otherwise), $\eta = Z_1 Z_2 e^2 / \hbar v$ is the Sommerfeld parameter, and $v = \sqrt{2E/\mu}$ is the relative

collision velocity (with kinetic center-of-mass energy E) at large separations. The factor $-2\pi\eta$ in the exponent argument comes from the definition of the astrophysical S factor [i.e., it determines the penetration through the pure Coulomb barrier $U_C^{(0)}(r) = Z_1 Z_2 e^2 / r$], and the factor $-E/k_B T$ comes from the Maxwellian distribution of reactants over E.

In the absence of plasma screening we have $R = R_0 = \chi n_1 n_1 I_0$, where the normalized reaction rate $I = I_0$ is

$$I_0 = \int_0^\infty dE \, S_0(E) \exp\left(-2\pi\eta - \frac{E}{k_B T}\right), \qquad (24)$$

and $S_0(E)$ is the standard astrophysical S factor calculated without any screening. In many cases the integral over E can be taken quite accurately using the saddle-point method, and this well-known result is

$$I_0 = 4\sqrt{\frac{2E_{p0}}{3\mu}} \frac{S_0(E_{p0})}{k_B T} \exp(-\tau), \qquad (25)$$

where $E_{p0} = k_B T \tau / 3$ is the Gamow-peak energy, and τ is given by Eq. (5).

Now we calculate Salpeter's rate, $R = R_S = \chi n_1 n_2 I_S$, including plasma screening under the following simplified assumptions:

(1) The screening potential is given by (22).
(2) The Coulomb barrier is thick; the barrier penetration is calculated in the WKB approximation.
(3) The barrier penetration is the same as in the s wave ($\ell = 0$).

The normalized reaction rate I_S is then given by the same equation (24) as I_0 but with $S_0(E)$ replaced by $S_S(E)$ to account for the plasma screening in Salpeter's model. The function $S_S(E)$ is determined by the quantum barrier penetration times $\exp(2\pi\eta)$, and the WKB penetration factor is (see Sec. VI)

$$\exp\left(-\frac{2}{\hbar} \int_{r_1}^{r_2} dr \sqrt{2\mu(U_{\text{eff}}(r) - E)}\right). \qquad (26)$$

In this case $U_{\text{eff}}(r)$ is the s-wave effective potential, which includes the nuclear and Coulomb components, while r_1 and r_2 are the classical inner and outer barrier penetration (turning) points, respectively. If we include Salpeter's screening, we have $U_{\text{eff}}(r) \to U_{\text{eff}}(r) - H_0$. Therefore, replacing $E \to E' = E + H_0$ we keep the expression for the factor (26) unchanged. With this in mind it is easy to show that

$$I_S = \int_0^\infty dE \, S_S(E) \exp\left(-2\pi\eta - \frac{E}{k_B T}\right) = f_S' I_S', \qquad (27)$$

with

$$I_S' = \int_{H_0}^\infty dE' \, S_0(E') \exp\left(-2\pi\eta(E') - \frac{E'}{kT}\right) \qquad (28)$$

and

$$f_S' = \exp\left(\frac{H_0}{k_B T}\right). \qquad (29)$$

In Eq. (27) we have introduced

$$S_S(E) = S_0(E + H_0) \exp[2\pi\eta(E) - 2\pi\eta(E + H_0)], \qquad (30)$$

which can be called Salpeter's S factor corrected for plasma screening effects (within Salpeter's model). Notice that Salpeter did not directly include plasma screening into $S(E)$ but his calculations can be treated in this way.

Now the enhancement factor f_S of nuclear reactions in Salpeter's model becomes

$$f_S = \frac{R_S}{R_0} = f'_S \frac{I'_S}{I_0}. \tag{31}$$

If the integral (28) can be calculated by the standard saddle-point method and the integrand function has a traditional Gamow-peak shape with the Gamow-peak window above H_0, we can shift the lower integration limit to 0 and immediately obtain $I'_S = I_0$. Then the enhancement factor acquires the standard Salpeter's form [9]

$$f_S = f'_S = \exp\left(\frac{H_0}{k_B T}\right) = \exp(\Gamma_{12} b_0). \tag{32}$$

In the regime of strong Coulomb coupling this factor can be huge.

As a byproduct of the saddle-point integration in Eq. (28) we obtain that the Gamow-peak energy in Salpeter's model is $E'_{pS} = E_{pS} + H_0 = E_{p0}$, and the outer turning point is unaffected by the screening. Then

$$E_{pS} = \frac{\tau k_B T}{3} - H_0, \quad r_2 = \frac{3 Z_1 Z_2 e^2}{k_B T \tau}. \tag{33}$$

Therefore, when the temperature decreases, E_{pS} goes down and (formally) can become negative. The Gamow-peak window moves then out of the integration region $E > 0$ in Eq. (27) and the saddle-pint method becomes inapplicable. The condition $E_{pS} = 0$ corresponds to $\zeta \approx 1$, with ζ defined by Eq. (5). At these low temperatures the thermonuclear reaction regime breaks down and the present formalism becomes questionable. Accordingly, in Fig. 1 we restrict the domain of thermonuclear burning by the $\zeta = 1$ line ($T \approx 0.34 T_p$, where the ion plasma temperature T_p is defined in Sec. II).

For illustration, Fig. 4 displays the effective potential $U_{\text{eff}}(r)$ for the $^{12}\text{C} + ^{12}\text{C}$ reaction in dense carbon matter (in the $\ell = 0$ channel) including the nuclear and Coulomb potentials. The solid line is the standard theoretical potential, which is taken from Ref. [23] and neglects plasma screening effects. It is almost a pure Coulomb potential at $r \gtrsim 9$ fm but it is strongly dominated by nuclear attraction at lower r. The three lower lines (long-dashed, dashed-dot, and short-dashed) are obtained by taking into account the plasma screening in the regime of strong Coulomb coupling (the dashed domain in Fig. 1) at $\rho = 10^8$, 10^9, and 10^{10} g cm^{-3}. The Coulomb part of $U_{\text{eff}}(r)$ is corrected for plasma screening. For the displayed conditions, Salpeter's Eq. (22) is an excellent approximation for $U_C(r)$. At $\rho = 10^8$, 10^9, and 10^{10} g cm^{-3} the plasma screening reduces the potential by $H_0 = 0.151$, 0.326, and 0.702 MeV, respectively. The higher the density, the stronger the screening effect (the larger the enhancement factor).

The thin vertical lines in Fig. 4 position the outer turning points r_2, Eq. (33), for the barrier penetration with the Gamow-peak energy at $T = 8 \times 10^8$, 4×10^8, and 2×10^8 K ($r_2 = 24.88$, 39.49, and 62.69 fm, respectively). The Gamow-peak energies for these temperatures are $E_{pS} = 2.08$, 1.31, and
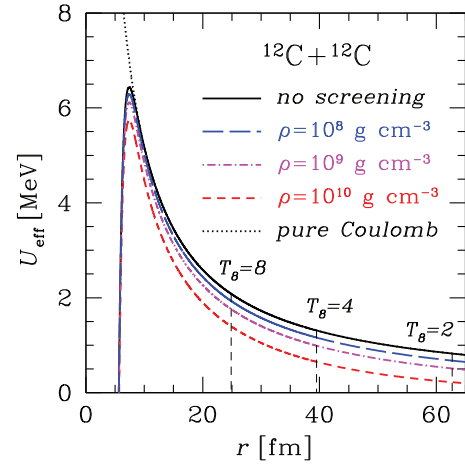

FIG. 4. (Color online) Effective potential for the $^{12}\text{C} + ^{12}\text{C}$ reaction in carbon matter. The solid line is the potential with plasma screening effects neglected. The long-dashed, dot-dashed, and short-dashed lines are the potentials reduced by plasma screening in the regime of strong Coulomb coupling at $\rho = 10^8$, 10^9, and 10^{10} g cm^{-3}, respectively. The dotted line is the pure Coulomb potential for pointlike nuclei. The three thin vertical lines position the outer turning point r_2, Eq. (33), for barrier penetration with the Gamow-peak energy E_{pS} in Salpeter's model at (from left to right) $T_8 = T/(10^8 \text{ K}) = 8$, 4, and 2, respectively. See text for details.

0.827 MeV. Figure 4 clearly shows the ranges of sub-barrier distances which regulate the barrier penetration in the WKB approximation. Only these distances are important for the nuclear reaction problem, and in all the displayed cases the Salpeter's potential (22) serves as a very good approximation. It would not be distinguishable from the exact screened potential in Fig. 4. At larger r, Salpeter's potential would be noticeably different from the exact one, especially at the highest assumed $\rho = 10^{10}$ g cm^{-3} (in which case the difference would be pronounced at $r \gtrsim 80$ fm). However, these large r could contribute to the nuclear reaction rates only at lower T at which our approach becomes invalid (where pycnonuclear effects, which we neglect, would become strong).

In Fig. 5 we show the astrophysical S factor for the $^{12}\text{C} + ^{12}\text{C}$ reaction in carbon matter as calculated in Salpeter's model from Eq. (30). The solid line is the standard theoretical S factor unaffected by plasma screening. The long-dashed, dot-dashed, and short-dashed lines are the S factors calculated with account for plasma screening at $\rho = 10^8$, 10^9, and 10^{10} g cm^{-3}, respectively. The screening effects increase the transparency of the Coulomb barrier in dense plasma (Fig. 4). These effects are especially pronounced at low energies E and high densities ρ where the S factor is enhanced by many orders of magnitude. Naturally it dramatically enhances nuclear reaction rates.

Figure 6 presents the $^{12}\text{C} + ^{12}\text{C}$ reaction rate in carbon matter as a function of temperature for the same three values of ρ. Again, the long-dashed, dot-dashed, and short-dashed lines refer to $\rho = 10^8$, 10^9, and 10^{10} g cm^{-3}, respectively. As seen from Fig. 1, the ranges of T and ρ chosen in Fig. 6 correspond to thermonuclear burning with strong plasma screening. The thin lines show the rates calculated with screening neglected.
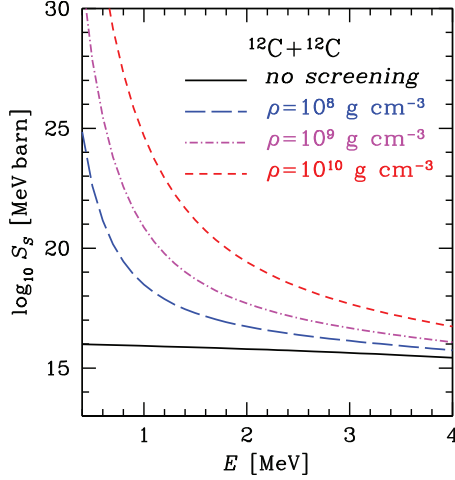
FIG. 5. (Color online) Astrophysical S factor as a function of the center-of-mass energy E of reactants for the ^{12}C + ^{12}C reaction in carbon matter calculated in Salpeter's model. The solid line is the standard S factor with plasma screening neglected. The long-dashed, dot-dashed, and short-dashed lines are the S factors enhanced by plasma screening in the regime of strong Coulomb coupling at $\rho = 10^8$, 10^9, and 10^{10} g cm^{-3}, respectively.

The thick lines include the screening in Salpeter's model. The screening always enhances the rate but does not prevent the decrease of the rate with the fall of T as long as the burning regime is thermonuclear (i.e., the rate becomes temperature independent only in the pycnonuclear regime). It is seen that the screening enhancement of the thermonuclear reaction rate increases at lower T. For $\rho = 10^8$ g cm^{-3} the screening effect is not very strong but at $\rho = 10^{10}$ g cm^{-3} and the lowest displayed $T \approx 1.5 \times 10^8$ K it is tremendous: it enhances the reaction rate by more than 20 orders of magnitude (also see Sec. VIII).
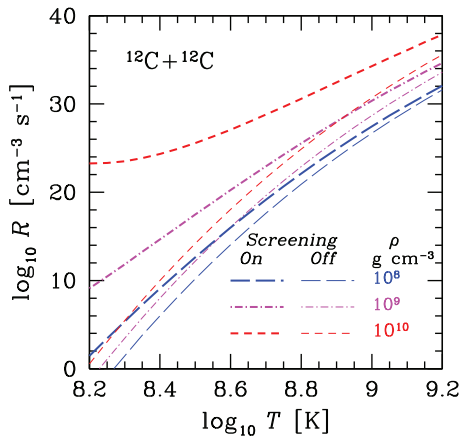

FIG. 6. (Color online) ^{12}C + ^{12}C thermonuclear reaction rate in carbon matter as a function of temperature. The long-dashed, dot-dashed, and short-dashed lines correspond to $\rho = 10^8$, 10^9, and 10^{10} g cm^{-3}, respectively. Thin lines are calculated with plasma screening neglected, while thick lines include the screening in Salpeter's model (see text for details).

VI. ASTROPHYSICAL S FACTOR

A. Screening effects on S factor

At the next step we use the liquid drop model and calculate astrophysical S factors and thermonuclear reaction rates beyond Salpeter's model.

In the barrier penetration model the astrophysical S factor is given by

$$S(E) = \exp(2\pi\eta)\frac{\pi\hbar^2}{2\mu}\sum_{\ell}(2\ell+1)T_\ell(E)P_\ell(E), \quad (34)$$

where η is defined in Sec. V, T_ℓ is the barrier penetration probability, P_ℓ is the nuclear fusion probability, and the sum is over angular momenta ℓ. For low energies of astrophysical interest it is usually sufficient to set $P_\ell(E) = 1$.

At sub-barrier energies the barrier penetration probability is small and can be described by the WKB formula

$$T_\ell(E) = \exp[-s_\ell(E)],$$

$$s_\ell(E) = \frac{2}{\hbar}\int_{r_1}^{r_2} dr\sqrt{2\mu\left(U_{\text{eff}}(r) + \frac{\hbar^2\ell(\ell+1)}{2\mu r^2} - E\right)}, \quad (35)$$

where $U_{\text{eff}}(r)$ is the effective potential at $\ell = 0$ (Fig. 4). The potential contains the standard potential, in which plasma screening is neglected, minus $H(r)$ given by Eqs. (10) and (20).

As discussed in Sec. V, one of the screening effects on $S(E)$ would be to shift $E \to E + H_0$, which corresponds to

$$S(E) \to S_0(E'), \quad E' = E + H_0. \quad (36)$$

Therefore, we can write

$$S(E) = S_0(E')q(E), \quad (37)$$

where $q(E)$ is an extra correction factor to be analyzed.

Introducing dimensionless units (Sec. II) we rewrite Eq. (35) as

$$s_\ell(\epsilon) = \frac{4\Gamma_{12}}{\pi\zeta^{3/2}}\int_{x_1}^{x_2} dx\sqrt{v(x) + \frac{\pi^2\zeta^3\,\ell(\ell+1)}{4\Gamma_{12}^2\,x^2} - \epsilon}, \quad (38)$$

where $v(x) = U_{\text{eff}}(r)/E_{12}$, $\epsilon = E/E_{12}$, and $x = r/a_{12}$, with $v(x) = 0$ and $h(x) = 1/x$ for $x \geqslant 2$.

According to Eq. (34) we can write

$$q(\epsilon) = q_0(\epsilon)q_L(\epsilon), \quad (39)$$

where $q_0(\epsilon)$ and $q_L(\epsilon)$ include the corrections due to $\ell = 0$ and $\ell > 0$ channels, respectively. Using (35), we have

$$q_0(\epsilon) = \exp(2\pi\eta - 2\pi\eta' - s_0 + s'_{00}) \quad (40)$$

and

$$q_L(\epsilon) = \frac{\sum_\ell(2\ell+1)\exp(s_0 - s_\ell)}{\sum_\ell(2\ell+1)\exp(s'_{00} - s'_{0\ell})}, \quad (41)$$

where summation is over all $\ell \geqslant 0$, $\eta = \eta(\epsilon)$, $\eta' = \eta(\epsilon')$, $s_\ell = s_\ell(\epsilon)$, and $s'_\ell = s_\ell(\epsilon')$, with s'_{00} and $s'_{0\ell}$ being the quantities calculated with screening neglected.

Evidently, the S factors are affected by nuclear physics and plasma physics effects. In the thermonuclear regime these

effects are usually decomposed and studied separately. We will mainly focus on the plasma screening effects, which are determined by differences like $s'_{00} - s_0$. They are expressed as integrals whose integrands are small at those conditions at which nuclear forces are significant. To analyze these integrals, it is sufficient that we neglect the nuclear potential in $U_{\rm eff}(r)$ in the expressions for $q(E)$, assuming thus $U_{\rm eff}(r) = U_C(r)$. In this approximation the inner turning point goes to zero: $r_1 \to 0$ ($x_1 \to 0$).

B. Screening correction in the *s* wave

Here we study the factor q_0 given by Eq. (40). We have

$$s_0 - s'_{00} = \Gamma_{12}\zeta^{-3/2}[F(\epsilon) - F_0(\epsilon')], \qquad (42)$$

where

$$F_0(\epsilon) = \frac{4}{\pi}\int_0^{x_{02}} dx\,\sqrt{\frac{1}{x}-\epsilon} = \frac{2}{\sqrt{\epsilon}}, \qquad (43)$$

$$F(\epsilon) = \frac{4}{\pi}\int_0^{x_2} dx\,G_\epsilon(x), \quad G_\epsilon(x) = \sqrt{\frac{1}{x}-h(x)-\epsilon}. \qquad (44)$$

The term $\Gamma_{12}\zeta^{-3/2}F_0(\epsilon')$ cancels $-2\pi\eta'$ in Eq. (40), so that

$$q_0(\epsilon) = \exp\{-\Gamma_{12}\zeta^{-3/2}[F(\epsilon) - F_0(\epsilon)]\}. \qquad (45)$$

The higher the energy ϵ (or ϵ'), the lower the turning point x_2 in Eq. (44). Therefore, we can derive the high-ϵ expansion corresponding to the small-x expansion (11). For this purpose we rewrite the integral (44) in the form

$$F(\epsilon) = \frac{4}{\pi}\int_0^\infty x_2(G^2+\epsilon')\,dG, \qquad (46)$$

where $x_2(\lambda)$ is the solution to the equation $\lambda - \epsilon' = 1/x_2 - h(x_2) - \epsilon$. Taking $\lambda = \epsilon'$ we see that $x_2(\epsilon')$ (at $G = 0$) is indeed the turning point x_2, justifying the notation. The equation for $x_2(\lambda)$ can be rewritten as

$$x_2 = \frac{1 - b_2 x_2^3 - b_4 x_2^5 - \cdots}{\lambda}, \qquad (47)$$

which is easily iterated to obtain the series expansion

$$x_2(\lambda) = \frac{1}{\lambda} - \frac{b_2}{\lambda^4} - \frac{b_4}{\lambda^6} + \frac{3b_2^2}{\lambda^7} + \cdots. \qquad (48)$$

Substituting it into Eq. (46) and integrating we obtain

$$F(\epsilon) = F_0(\epsilon')\left[1 - \frac{5b_2}{16\,\epsilon'^3} - \frac{63b_4}{256\,\epsilon'^5} + \frac{693b_2^2}{1024\,\epsilon'^6} + \cdots\right]. \qquad (49)$$

We have not rigorously examined the convergence of this series, but it seems asymptotic. In any case, for the low energies of interest, the higher-order terms do not considerably increase the accuracy. Thus we can safely omit the last term.

To have an accurate expression for $F(\epsilon)$ we also have calculated $F(\epsilon)$ numerically and fitted the results by

$$F(\epsilon) = F_0(\epsilon')\left[1 - \frac{5b_2}{16\,\epsilon'^3} - c_1\frac{63b_4}{256\,\epsilon'^5} + c_2\frac{693b_2^2}{1024\,\epsilon'^6}\right], \qquad (50)$$

where $c_1 = 3.662$ and $c_2 = 2.762$ are two fit parameters. The ranges of ϵ and z employed in the fit are $0.00025 \lesssim \epsilon \lesssim 9$ and $1 \leqslant z \leqslant 10$. The maximum relative fit error is 1.6% (at $z = 1$ and $\epsilon \approx 0.00025$) and the absolute rms error is 10^{-4}. For $0.05 \leqslant \epsilon \leqslant 2.0$ and the same z the maximum relative error is 0.6%. Nevertheless, we will not use this fit formula further but restrict ourselves by the analytic expansion (49).

Note that Eq. (45) with $F(\epsilon) = F_0(\epsilon')$ corresponds to Salpeter's model, while the bracketed factors in Eqs. (49) and (50) are the corrections provided by the electron drop model.

C. Screening correction due to higher-ℓ waves

Here we analyze the factor $q_L(\epsilon)$ which is given by Eq. (41) and provides the screening correction to $S(E)$ due to $\ell \geqslant 1$ reaction channels.

We expand (38) in powers of centrifugal energy, keeping the first-order term:

$$s_0(\epsilon) - s_\ell(\epsilon) = -\frac{\pi\zeta^{3/2}\ell(\ell+1)}{\Gamma_{12}}\,g(\epsilon), \qquad (51)$$

where

$$g(\epsilon) = \int_{x_1}^{x_2}\frac{dx}{2x^2\sqrt{v(x)-\epsilon}}. \qquad (52)$$

Higher-order terms in (51) are suppressed by extra powers of Γ_{12}^{-1}. In this approximation the turning points x_1 and x_2 in $g(\epsilon)$ are the same as for the *s* wave. Now we treat the exponent arguments in (41) as small and replace the sums by integrals. It turns out to be a good approximation for the ratio (but a poorer approximation for the sums themselves). We obtain

$$q_L(\epsilon) = \frac{g_0(\epsilon')}{g(\epsilon)} = \frac{g_0(\epsilon')}{g_0(\epsilon') + \delta g(\epsilon)}, \qquad (53)$$

where $g_0(\epsilon)$ is given by the same Eq. (52) as $g(\epsilon)$ but with plasma screening neglected and $\delta g(\epsilon) = g(\epsilon) - g_0(\epsilon')$. The function $\delta g(\epsilon)$ can be calculated by neglecting the nuclear interaction and taking $x_1 \to 0$. In this approximation it is universal—independent of a particular reaction. The function $g_0(\epsilon)$ is independent of plasma screening; it can be calculated for a given reaction by using a suitable model of the nuclear interaction (for instance, employing the same formalism as in Refs. [23,24]).

In analogy to (49), we have derived a high-ϵ expansion for δg:

$$\delta g(\epsilon) = -\frac{3\pi b_2}{8\epsilon'^{5/2}} - \frac{35\pi b_4}{64\epsilon'^{9/2}} + \frac{315\pi b_2^2}{256\epsilon'^{11/2}} + \cdots. \qquad (54)$$

Let us restrict ourselves to $\zeta \leqslant 1$. For $\zeta = 1$ and $z = 1$ the Gamow-peak energy is about $\epsilon_p \simeq 0.24$ [see Eq. (60) below]. In this case the above expansion gives $\delta g \simeq 0.19$, while the integral (52) gives $\delta g \simeq 0.21$. For smaller ζ and higher ϵ_p the expansion is even more exact.

While $0 < \delta g \lesssim 0.2$–0.3, g_0 is typically greater than one. To verify the last statement we have taken the reaction database from Ref. [24]. It contains about 5,000 reactions involving stable and unstable isotopes of 10 elements (Be, B, C, N, O, F, Ne, Na, Mg, and Si). We have checked directly that $g_0 \gtrsim 1$ for the reactions between nuclei which are close

to the stability valley at those densities and temperatures where Gamow-peak energies are lower than barrier hight (for otherwise the reactions are so fast that the nuclei do not exist in dense matter). Therefore, for many reactions of practical interest q_L does not deviate from $q_L = 1$ by more than $\sim 20\%$, which is well within expected uncertainties in the S factors and reaction rates. To avoid unnecessary complications we suggest disregarding screening corrections due to higher-ℓ waves and set $q_L = 1$.

VII. PLASMA SCREENING ENHANCEMENT OF REACTION RATES

As seen from Eq. (23), the plasma screening enhancement factor of the thermonuclear reaction rate is

$$f = I/I_0, \qquad (55)$$

where I, expressed in our dimensionless units (Sec. II), is given by

$$I = E_{12} \int_0^\infty S_0(\epsilon') \exp[-\Gamma_{12}(\zeta^{-3/2}F(\epsilon) + \epsilon)]\, d\epsilon. \qquad (56)$$

Generally, one can calculate f numerically from Eq. (55). Instead, we analyze f analytically by employing the traditional Gamow-peak formalism. With decreasing temperature, the Gamow peak becomes narrower, which makes the formalism more accurate. On the other hand, the peak energy decreases, and at $\zeta \approx 1$ (i.e., at $T \approx 0.34\, T_p$) the peak energy goes to zero (Sec. V), which manifests the breakdown of the thermonuclear burning regime and the transition to pycnonuclear burning. We will restrict ourselves to $\zeta \lesssim 1$; at higher ζ the present formalism can be considered as an approximation.

In the Gamow-peak formalism we can decompose f as

$$f = f_{\text{scr}} f_{S\text{fact}}, \qquad (57)$$

where f_{scr} is calculated from Eq. (55) by neglecting the dependence of the astrophysical S factor on energy ϵ, while

$$f_{S\text{fact}} = S_0(\epsilon_p')/S_0(\epsilon_{p0}) \qquad (58)$$

takes into account that plasma screening (beyond Salpeter's model) shifts the Gamow peak (from ϵ_{p0} to ϵ_p).

We will mainly focus on f_{scr} and discuss $f_{S\text{fact}}$ briefly in Sec. VIII. It is traditional to express f_{scr} as

$$f_{\text{scr}} = \exp[h_0(\Gamma_{12}) + h_1(\Gamma_{12}, \zeta)]. \qquad (59)$$

Here, $h_0(\Gamma_{12}) = \Gamma_{12} b_0 = H(0)/(k_B T)$ is the leading term of the normalized screening potential $h(x)$. This term includes quantum tunneling in a Coulomb potential lowered by a constant value $H(0)$ (equivalent to Salpeter's approximation; Sec. V). This term does not change the Coulomb potential shape, and therefore it does not affect the dynamics of quantum tunneling. The next term $h_1(\Gamma_{12}, \zeta)$ in the exponent of Eq. (59) is the correction to $h_0(\Gamma_{12})$; it is produced by the variation of the mean-field potential shape due to screening over the quantum tunneling path; it is generally smaller than $h_0(\Gamma_{12})$.

Let us take Eq. (56) and use the expansion (49) (treating the $1/\epsilon'^3$ and $1/\epsilon'^5$ terms in the parentheses as small corrections and neglecting the $1/\epsilon'^6$ term). Furthermore, we ignore the dependence of S_0 on ϵ, and we take the integral I by the
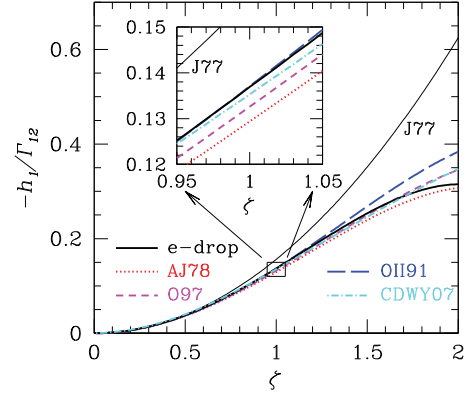

FIG. 7. (Color online) The function $-h_1(\Gamma_{12}, \zeta)/\Gamma_{12}$ vs ζ in the regime of strong Coulomb coupling at $Z_1 = Z_2$. The thin solid line (J77) corresponds to the leading term of Eq. (61) derived by Jancovici [13]; thick lines of various types are calculations by different authors (AJ78: [25]; O97: [26]; OII91: [14]; CDWY07: [22]; e-drop: present work). The insert is an expansion showing the behavior of the different curves at $\zeta \approx 1$ (see text for details).

standard saddle-point method. This gives the dimensionless Gamow-peak energy

$$\epsilon_p' = \frac{1}{\zeta} + \delta\epsilon_p, \quad \delta\epsilon_p = -\frac{35}{24} b_2 \zeta^2 - \frac{231}{128} b_4 \zeta^4. \qquad (60)$$

The leading term $1/\zeta$ corresponds to Salpeter's approximation [see Eqs. (6) and (33)], while $\delta\epsilon_p$ is a small correction beyond this approximation.

With such a correction the saddle-point method gives

$$h_1(\Gamma_{12}, \zeta) = \Gamma_{12}\left(\tfrac{5}{8} b_2 \zeta^2 + \tfrac{63}{128} b_4 \zeta^4\right). \qquad (61)$$

Equations (60) and (61) represent truncated expansions in powers of ζ. Higher-order terms (starting with ζ^5) can be determined but seem unimportant for applications. The advantage of these equations is that they are derived from first principles. They are valid for any mean-field screening potential (not only for the electron drop model). In order to use them one needs the three coefficients b_0, b_2, and b_4, for a given mean-field model. Note that the leading term in $h_1(\Gamma_{12}, \zeta)/\Gamma_{12}$ is $\tfrac{5}{8} b_2 \zeta^2$; it is well known [25]; the second term seems original.

By way of illustration, in Fig. 7 we present the function $h_1(\Gamma_{12}, \zeta)/\Gamma_{12}$ versus ζ at $Z_1 = Z_2$ and strong Coulomb coupling as calculated by several authors. The insert shows details of the behavior of the different curves at $\zeta \approx 1$. The thin solid curve J77 shows the leading term in Eq. (61); it was derived by Jancovici [13]. The thick solid curve (e-drop) is our electron drop model; the dotted curve AJ78 is derived by Alastuey and Jancovici [25]; the short-dashed curve O97 is by Ogata [26]; the long-dash curve OII91 is by Ogata, Iyetomi and Ichimaru [14]; and the dot-dashed curve CDWY07 is by Chugunov, DeWitt and Yakovlev [22]. In the electron drop model $h_1(\Gamma_{12}, \zeta)/\Gamma_{12}$ is independent of Γ_{12}. For other models it is a slowly varying function of Γ_{12}. In these cases, we set $\Gamma_{12} = 150$. Although the present formalism is strictly valid at $\zeta \lesssim 1$, we extend the plot to $\zeta = 2$ to demonstrate the diversity of results by different authors. These results are

TABLE I. Parameters of electron drop and combined models.

Model	b_0	b_2	b_4
Electron drop	Eq. (13)	Eq. (14)	Eq. (15)
Combined	Eq. (18)	Eq. (14)	Eq. (15)

usually presented as analytic fits to numerical calculations by various methods. We see that our analytic Eq. (61) at $\zeta \lesssim 1$ agrees very well with other results. The divergency of the results at $\zeta \gtrsim 2$ is unimportant for us because we restrict ourselves to the thermonuclear reaction regime at $\zeta < 1$.

VIII. DISCUSSION

The main practical outcome of our consideration is that the enhancement factor of a nonresonant fusion reaction due to strong plasma screening is given by Eqs. (59) and (61). Combined with $h_0(\Gamma_{12}) = \Gamma_{12}b_0$, these equations give

$$f_{\mathrm{scr}} = \exp\left[\Gamma_{12}\left(b_0 + \tfrac{5}{8}b_2\zeta^2 + \tfrac{63}{128}b_4\zeta^4\right)\right], \quad (62)$$

expressing f_{scr} through three coefficients ($b_0, b_2,$ and b_4) which can be slowly varying functions of plasma parameters and charge numbers Z_1 and Z_2 of the reactants. This formula is derived from first principles in the mean-field approximation; it is expected to be valid for any mean-field model of the screening potential. Its applicability is restricted by strong screening ($\Gamma_{12} \gtrsim 1$; $T \lesssim T_l$ in Fig. 1) and the thermonuclear burning regime ($\zeta \lesssim 1$; $T \gtrsim 0.34\,T_p$ in Fig. 1). The b_0 (Salpeter's) term in Eq. (62) is leading while other terms are relatively less important.

We can point out two mean-field models of the screening potential: the electron drop model and the model which we call combined. The former is simple and uniform while the latter is more accurate. Their parameters are listed in Table I.

In the electron drop model, b_0, b_2, and b_4 depend on $z = Z_2/Z_1$ but are independent of density and temperature. These coefficients are given by Eqs. (13)–(15). The main disadvantage of this model is that b_0 is actually a slowly varying function of the Coulomb coupling parameter, which is neglected.

In the combined model, b_0 is given by Eq. (18), while b_2 and b_4 are again given by Eqs. (14) and (15). Equation (18) is based on extensive MC simulations and is, therefore, more accurate than (13); Eq. (14) provides a robust value of b_2 (Sec. IV), while b_4 is relatively unimportant, so that the use of the electron drop value (15) is sufficiently accurate.

In Fig. 8 we illustrate the efficiency of the plasma screening as a function of temperature for the $^{12}\mathrm{C} + ^{12}\mathrm{C}$ reaction in carbon matter at $\rho = 10^{10}\,\mathrm{g\,cm^{-3}}$ (also see Fig. 6 to understand how this efficiency affects the reaction rate). At the highest displayed temperature, we have $\log_{10} T\,[\mathrm{K}] = 9.6$, $\Gamma_{12} \approx 2$, and $\zeta \approx 0.1$, while at the lowest temperature $\log_{10} T\,[\mathrm{K}] = 8.15$, $\Gamma_{12} \approx 55$, and $\zeta \approx 1$.

We present the four curves which correspond to different models and approximations. The thin short-dashed curve refers to Salpeter's model where only the h_0 term is included in Eq. (59), with b_0 given by Eq. (13). This is equivalent to
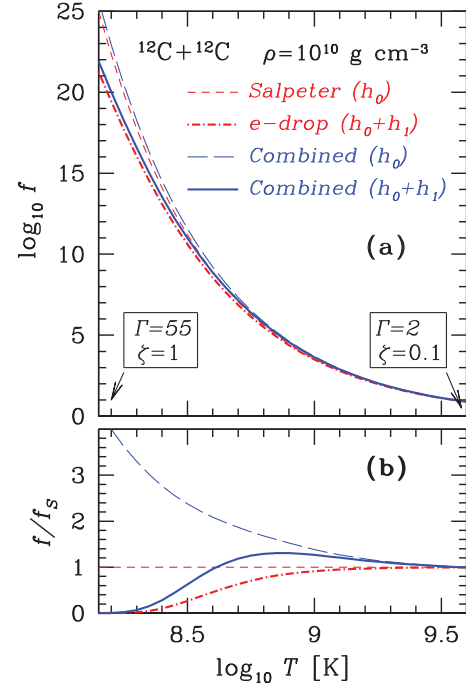

FIG. 8. (Color online) Enhancement of the $^{12}\mathrm{C} + ^{12}\mathrm{C}$ thermonuclear reaction rate in carbon matter at $\rho = 10^{10}\,\mathrm{g\,cm^{-3}}$ as a function of temperature. (a) Logarithm of the enhancement factor in Salpeter model [short-dashed line, with only h_0 included in Eq. (59)], the electron drop model (dot-dash line, with h_0 and h_1 included), and in the combined model including and excluding h_1 (solid and long-dashed lines, respectively). The numbers give the values of $\Gamma = \Gamma_{12}$ and ζ at the lowest and highest temperatures displayed. (b) The same enhancement factors divided by Salpeter's factor on a linear scale (see text for details).

using Eq. (62), where the b_2 and b_4 terms are dropped. The thick dot-dashed curve is for the full electron drop model [h_0 and h_1 terms are included in Eq. (59); all terms are included in Eq. (62)]. The thin long-dash curve is similar to Salpeter's model but b_0 is given by Eq. (18). The thick solid curve is the full combined model [all terms included in Eq. (59) or (62)].

Figure 8(a) shows the logarithm of f while Fig. 8(b) presents f/f_S on a linear scale for the four approximations. When the temperature drops to $\log_{10} T = 8.15$ the plasma screening enhancement intensifies and exceeds 20 orders of magnitude. It greatly slows down the decrease of the thermonuclear reaction rate (cf. Fig. 6). As long as $\zeta \ll 1$ ($T \gtrsim 10^9$ K, for a given $\rho = 10^{10}\,\mathrm{g\,cm^{-3}}$), the screening enhancement is mainly provided by Salpeter's term (h_0). However, at lower T the correction h_1 becomes progressively more important. It suppresses Salpeter's screening enhancement (by about three orders of magnitude at $\log_{10} T \approx 8.15$ in Fig. 8). In this way it does not allow the plasma screening enhancement at low temperatures to become too strong (for otherwise the reaction rate would start growing with the temperature fall). It looks as if the h_1 correction "anticipates" the onset of the pycnonuclear burning regime at lower temperatures and "prepares" the temperature independence

of the reaction rate in the pycnonuclear regime. This independence of temperature at lowest temperatures of thermonuclear burning has been obtained earlier by Chugunov and DeWitt [16] (who calculated the plasma screening enhancement factors based on extensive MC calculations of screening potentials).

Neglecting the h_1 term, we would obtain [Fig. 8(b)] a factor of 4 difference of the enhancement factors in Salpeter's model and the combined model at the lowest T. Although this difference can be regarded as substantial, it is actually not very important for two reasons. First, the enhancement factors become huge by themselves [and the difference by a factor of 4 is really insignificant; see Fig. 8(a)]. Second, the inclusion of the h_1 correction strongly affects the plasma screening enhancement at lowest temperatures and reduces this difference. Therefore, even if the combined screening model is more accurate than the electron drop one, the difference does not seem important for applications.

Our final result, Eq. (62), is obtained by neglecting the energy dependence of the astrophysical factor S_0. This approximation corresponds to $f_{Sfact} = 1$ in Eq. (57). We have checked the validity of this assumption for the $^{12}C + ^{12}C$ reaction at $\rho = 10^{10}$ g cm^{-3} as an example, by using Eq. (58) for calculating f_{Sfact} and Eq. (60) for finding the shift of the Gamow-peak energy. This shift appears to be relatively small; f_{Sfact} stays smaller but fairly close to 1 for all temperatures displayed. The maximum difference (of about 5%) from $f_{Sfact} = 1$ occurs at the lowest temperature $\log_{10} T = 8.15$ shown in Fig. 8. Therefore, $f_{Sfact} = 1$ is, indeed, a good approximation.

Let us stress that nuclear reaction rates in stellar matter are also uncertain due to rather poor knowledge of the factors S_0 at low energies of astrophysical interest; see, e.g., Ref. [24] and references therein. These factors are difficult to calculate accurately and to measure in the laboratory; they may have resonant behavior which requires special consideration (even if the strengths and positions of resonances were known—which is usually not the case; see, e.g., Refs. [27,28] in which the $^{12}C + ^{12}C$ reaction is analyzed at low energies).

We add that we have studied plasma screening effects under the assumption of a rigid (incompressible) electron background. The corrections due to finite polarizability of the electron gas slightly increase the screening enhancement (see, e.g., Refs. [29,30], and references therein), which we neglect here.

All these factors prevent exact calculation of thermonuclear reaction rates in dense stellar matter. However, in many cases the exact rates are not vitally important because of the strong temperature dependence of the rates—their uncertainties are easily absorbed by small temperature variations, making modeling of nuclear burning phenomena almost unchanged (see, e.g., Ref. [31]).

We have not focused on plasma screening of thermonuclear reactions in the regime of weak Coulomb coupling ($T \gtrsim T_l$ in Fig. 1). One can use our formulas in this regime; they would predict weak plasma screening, $f \rightarrow 1$. Although such a description of weak screening is approximate, it should not noticeably affect physical results. More reliable plasma screening corrections for weak and moderate Coulomb

coupling can be obtained by using recent advances in this field [32–34].

At low temperatures ($\zeta \gtrsim 1$, $T \lesssim 0.34\,T_p$ in Fig. 1) the present results [Eq. (62)] become invalid because of the onset of the pycnonuclear burning regime. Pycnonuclear burning has been studied in many publications (e.g., Refs. [1,16,22] and references therein) but we believe that the theory of pycnonuclear reactions is still far from being complete.

IX. CONCLUSIONS

We have developed a simple model for plasma screening in thermonuclear reactions in dense stellar matter. In this model, the screening is produced by an electron cloud around the reacting nuclei. The cloud's charge is assumed to compensate for the charge of the reactants and the cloud's shape corresponds to the minimum electrostatic energy of the reacting system (two nuclei+electron cloud). This model is the extension of the well-known Salpeter's model of ion spheres [9].

The electron drop model is based on the mean-field screened Coulomb potential $H(r)$, which has been calculated for different nuclear charge numbers Z_1 and Z_2 (Sec. IV). We have analyzed the low-r expansion of $H(r)$ in powers of r^2 and derived (for the first time) the r^4 expansion term, Eq. (15). We have computed $H(r)$ and obtained a simple fit, Eq. (20). In passing, we have calculated $H(r)$ for the model in which the electron cloud is approximated by a prolate Maclaurin ellipsoid (Appendix B).

At the next step we have added the plasma screening Coulomb potential to the total effective potential $U_{eff}(r)$, which governs nuclear reaction. With this new potential we have calculated the astrophysical S factors (Sec. VI). Our generalized S factors include the effects of nuclear and plasma screening interactions on the same footing. In the regime of strong Coulomb coupling of atomic nuclei in dense matter, they depend on the density of the matter, ρ. We have analyzed the properties of such S factors and presented simple analytic approximations. These generalized S factors are strongly modified by plasma screening at low energies E and high densities ρ. For "ordinary" nuclear reactions such as $^{12}C + ^{12}C$ the inclusion of plasma screening into S factors is equivalent to introducing traditional plasma screening enhancement factors in the reaction rates. However, generalized S factors would be more natural for those reactions for which the effective plasma screening length is comparable to the sizes of the reacting nuclei. Such reactions could occur at high temperatures in the inner crust of neutron stars; nuclear and plasma physics effects would be not separated there.

Finally, we have used the electron drop model and calculated thermonuclear reaction rates, studied their plasma screening enhancement, and approximated the enhancement factors by analytic expressions (Sec. VII). We have analyzed the properties of plasma screening enhancement and proposed a combined analytic model for strong plasma screening in thermonuclear reactions (Sec. VIII).

Our results are in good agreement with those obtained by other techniques. The advantage of our model is that it is well formulated, physically transparent, and easily formalized in

terms of analytic approximations at every step of investigation (for the effective potentials, astrophysical S factors, and enhancement factors of nuclear reactions). The results can be used to model various astrophysical manifestations of nuclear burning and nucleosynthesis in white dwarfs and neutron stars.

Strictly, our results cannot be used in the thermonuclear regime with weak plasma screening (high temperatures and low densities) but in that case the plasma screening has almost no effect on the reaction rates. Equally, the results are inapplicable at very low temperatures and high densities, where the pycnonuclear effects (zero-point vibrations of the reacting nuclei) become pronounced.

So far almost all the calculations of the reaction rates in dense matter have been performed within the mean-field potential. However, the plasma potential created by neighboring plasma particles is actually fluctuating (depending on the specific configuration of neighboring particles). Our model can be generalized to the case of fluctuating potential by introducing an ensemble of electron drops (of different shapes) around the reactants and probabilities of their realizations. This can offer perspective on the study of the effect of plasma field fluctuations on the reaction rates in dense matter.

APPENDIX A: COULOMB ENERGY

In the Appendices we show how to derive the first three coefficients b_0, b_2, and b_4 in the small-x expansion (11) of the screening potential in the electron drop model (Sec. III). To obtain these coefficients the shape of the electron drop can be approximated by a prolate Maclaurin ellipsoid for which the electrostatic problem is solved analytically (see, e.g., Ref. [35]). First, we define the main quantities, then present the equations for the Maclaurin ellipsoid (Appendix B) and build the desired expansion (Appendix C). Here we use standard physical units.

At $r \leqslant (a_1 + a_2)$ the Coulomb potential $U_C(r)$ in Eq. (7) can be written as

$$U_C(r) = \frac{Z_1 Z_2 e^2}{r} + W(r) - W_{12}, \quad W(r) = W_{ee}(r) + W_{ei}(r),$$
(A1)

where $W(r)$ is the electrostatic energy of the drop (excluding direct Coulomb interaction of pointlike ions). It contains the interaction energy of the ions (positioned at $\boldsymbol{r}_1$ and $\boldsymbol{r}_2$) with the electron drop,

$$W_{ei}(r) = Z_1 e \Phi(\boldsymbol{r}_1) + Z_2 e \Phi(\boldsymbol{r}_2),$$
(A2)

and the electrostatic energy of the drop,

$$W_{ee}(r) = -\frac{en_e}{2} \int_V dV\, \Phi(\boldsymbol{r}).$$
(A3)

In this case

$$\Phi(\boldsymbol{r}) = -en_e \int_V \frac{dV'}{|\boldsymbol{r} - \boldsymbol{r}'|}$$
(A4)

is the electrostatic potential created by the drop. The integration in Eqs. (A3) and (A4) is carried over the volume V of the electron drop confined within the surface $\partial V = S(r)$. The term W_{12} in Eq. (A1) is given by Eq. (9); it is introduced to satisfy the condition $U_C(r) = 0$ at $r \geqslant (a_1 + a_2)$ (Sec. III).

At $r \leqslant (a_1 + a_2)$ the screening energy $H(r)$ in Eq. (7) is given by

$$-H(r) = W(r) - W_{12}.$$
(A5)

APPENDIX B: MACLAURIN ELLIPSOID MODEL

At small r we approximate the electron drop by a Maclaurin ellipsoid prolate along the z axis. The radial coordinate $r_s(\theta)$ of the surface S is then given by

$$\frac{1}{r_s^2(\theta)} = \frac{\cos^2 \theta}{a_\parallel^2} + \frac{\sin^2 \theta}{a_\perp^2},$$
(B1)

where $a_\parallel$ and $a_\perp$ are the ellipsoid semiaxes (along the z axis and in the perpendicular plane, respectively) and θ is the polar angle.

The electron charge within the ellipsoid should compensate for the charge of the ions. This gives

$$Z_c = \frac{4\pi}{3} a_\parallel a_\perp^2 n_e = \frac{a_\parallel a_\perp^2}{a_e^3};$$
(B2)

a_e and Z_c are defined in Sec. II. Introducing the ellipticity of the ellipsoid, $\epsilon = \sqrt{1 - (a_\perp/a_\parallel)^2}$, we have

$$a_\parallel = a_c (1 - \epsilon^2)^{-1/3}, \quad a_\perp = a_c (1 - \epsilon^2)^{1/6},$$
(B3)

where a_c is given by Eq. (4).

The potential $\Phi(\boldsymbol{r})$ within the ellipsoid is

$$\Phi(\boldsymbol{r}) = -\pi e n_e (I - A_\parallel z^2 - A_\perp x^2 - A_\perp y^2),$$
(B4)

with

$$A_\parallel = 2 \frac{1 - \epsilon^2}{\epsilon^2} (L - 1), \quad L = \frac{1}{2\epsilon} \ln\left(\frac{1 + \epsilon}{1 - \epsilon}\right),$$
(B5)

$I = 2a_\perp^2 L$, and $A_\perp = 1 - A_\parallel/2$. Integrating the potential $\Phi(\boldsymbol{r})$ one obtains the Coulomb energy of the electron drop,

$$W_{ee} = \frac{3}{5} \left(\frac{4\pi}{3}\right)^2 e^2 n_e^2 a_\perp^4 a_\parallel L.$$
(B6)

In our case the ions are placed at the z axis, so that

$$W(r) = -\pi e^2 n_e \left[Z_c I - Z_1 A_\parallel z_1^2 - Z_2 A_\parallel z_2^2 \right] + W_{ee}.$$
(B7)

These formulas give $U_C(r)$ for any electron drop in the form of Maclaurin ellipsoid.

APPENDIX C: SMALL-r EXPANSION

At $r \ll (a_1 + a_2)$ the electron drop shape is well approximated by an ellipsoid with ellipticity $\epsilon \ll 1$. From Eq. (B1)

the shape becomes

$$r_s(\theta) = a_c \left(1 + \tfrac{1}{3}\epsilon^2 P_2(\cos\theta)\right), \tag{C1}$$

where $P_2(x) = \tfrac{1}{2}(3x^2 - 1)$. Higher-order terms are unimportant for our problem.

In the expression for the electrostatic energy, we expand $A_\parallel$, I, and W_{ee} in powers of ϵ^2, keeping first- and second-order terms, and obtain

$$A_\parallel = \frac{2}{3} - \frac{4}{15}\epsilon^2 - \frac{4}{35}\epsilon^4, \tag{C2}$$

$$I = 2a_c^2 \left(1 - \frac{1}{45}\epsilon^4\right), \tag{C3}$$

$$W_{ee} = \frac{4\pi}{5} Z_c e^2 n_e a_c^2 \left(1 - \frac{1}{45}\epsilon^4\right). \tag{C4}$$

Placing the coordinate origin in the center of the electron drop, we have

$$z_1 = -Z_2 r/Z_c, \quad z_2 = Z_1 r/Z_c. \tag{C5}$$

Now ϵ is the only free parameter. We will see that $\epsilon \propto r$; accordingly, we expand $W(r)$, keeping the terms r^4, ϵ^4, and $\epsilon^2 r^2$, which gives

$$W(r) = 2\pi a_c^2 e^2 n_e \left[-\frac{3Z_c}{5} + \frac{3Z_c \epsilon^4}{225} \right.$$
$$\left. + \frac{Z_1 Z_2 x^2}{3Z_c} - \frac{2Z_1 Z_2 x^2 \epsilon^2}{15Z_c}\right], \tag{C6}$$

where $x = r/a_c$. The optimal value of ϵ is found by minimizing $W(r)$, which gives

$$\epsilon^2 = 5Z_1 Z_2 x^2 / Z_c^2. \tag{C7}$$

At this ϵ,

$$W(r) = \frac{e^2}{a_e}\left[-0.9\,Z_c^{5/3} + \frac{Z_1 Z_2}{2Z_c}\left(\frac{r}{a_e}\right)^2 - \frac{Z_1^2 Z_2^2}{2Z_c^{11/3}}\left(\frac{r}{a_e}\right)^4\right]. \tag{C8}$$

Substituting this into Eq. (A1), we reproduce Eq. (11).

We have derived the interaction energy for a specific choice of the ellipsoid center; it satisfies the minimum energy requirement with respect to variations of ϵ. Now we sketch the proof that this solution is exact up to the r^5 order and minimizes energy with respect to any perturbations of the drop's shape.

Note that the minimum energy requirement is equivalent to the condition of constant (zero) total potential on the S surface. We have explicitly checked that this condition is satisfied. Moreover, we find that the potential induced by the ion charges and the *unperturbed* electron spherical drop on the surface of the *exact perturbed* electron drop is $\sim r^2$. It is important that the shape is spherical in the r order (with our specific choice of the coordinate origin). Therefore the deviation of the perturbed surface from the unperturbed one is $\sim r^2$. Since the potential mentioned above is $\sim r^2$, the shape correction $\sim r^3$ contributes only to the energy corrections $\sim r^5$ and higher. However, it is easily seen that there are no odd-order energy terms; hence the expansion is correct up to the terms $\sim r^5$. The absence of the odd-order terms is intuitively obvious, because all the intermediate equations respect the symmetry transformation $r \to -r$, $\theta \to \pi - \theta$, and θ is then integrated out in order to obtain the energy. Note that this symmetry is consistent with the Widom expansion [36].

---

[1] E. E. Salpeter and H. M. Van Horn, Astrophys. J. **155**, 183 (1969).

[2] S. L. Shapiro and S. A. Teukolsky, *Black Holes, White Dwarfs, and Neutron Stars* (Wiley-Interscience, New York, 1983).

[3] P. Höflich, Nucl. Phys. A **777**, 579 (2006).

[4] M. H. van Kerkwijk, P. Chang, and S. Justham, Astrophys. J. **722**, L157 (2010).

[5] H. Schatz, L. Bildsten, and A. Cumming, Astrophys. J. **583**, L87 (2003).

[6] A. Cumming, J. Macbeth, J. J. M. in 't Zand, and D. Page, Astrophys. J. **646**, 429 (2006).

[7] S. Gupta, E. F. Brown, H. Schatz, P. Möller, and K.-L. Kratz, Astrophys. J. **662**, 1188 (2007).

[8] E. M. Burbidge, G. R. Burbidge, W. A. Fowler, and F. Hoyle, Rev. Mod. Phys. **29**, 547 (1957).

[9] E. E. Salpeter, Aust. J. Phys. **7**, 373 (1954).

[10] P. Haensel, A. Y. Potekhin, and D. G. Yakovlev, *Neutron Stars. 1. Equation of State and Structure* (Springer, New York, 2007).

[11] L. R. Gasques, A. V. Afanasjev, E. F. Aguilera, M. Beard, L. C. Chamon, P. Ring, M. Wiescher, and D. G. Yakovlev, Phys. Rev. C **72**, 025806 (2005).

[12] Y. Rosenfeld and G. Chabrier, J. Stat. Phys. **89**, 283 (1997).

[13] B. Jancovici, J. Stat. Phys. **17**, 357 (1977).

[14] S. Ogata, H. Iyetomi, and S. Ichimaru, Astrophys. J. **372**, 259 (1991).

[15] A. Y. Potekhin and G. Chabrier, Phys. Rev. E **62**, 8554 (2000).

[16] A. I. Chugunov and H. E. DeWitt, Phys. Rev. C **80**, 014611 (2009).

[17] N. Itoh, N. Tomizawa, S. Wanajo, and S. Nozawa, Astrophys. J. **586**, 1436 (2003).

[18] N. Itoh, F. Kuwashima, and H. Munakata, Astrophys. J. **362**, 620 (1990).

[19] J.-M. Caillol and D. Gilles, J. Phys. A **36**, 6243 (2003).

[20] H. DeWitt and W. Slattery, Contrib. Plasma Phys. **39**, 97 (1999).

[21] J.-M. Caillol, J. Chem. Phys. **111**, 6538 (1999).

[22] A. I. Chugunov, H. E. DeWitt, and D. G. Yakovlev, Phys. Rev. D **76**, 025028 (2007).

[23] D. G. Yakovlev, M. Beard, L. R. Gasques, and M. Wiescher, Phys. Rev. C **82**, 044609 (2010).

[24] A. V. Afanasjev, M. Beard, A. I. Chugunov, M. Wiescher, and D. G. Yakovlev, Phys. Rev. C **85**, 054615 (2012).

[25] A. Alastuey and B. Jancovici, Astrophys. J. **226**, 1034 (1978).

[26] S. Ogata, Astrophys. J. **481**, 883 (1997).

[27] E. F. Aguilera *et al.*, Phys. Rev. C **73**, 064601 (2006).

[28] T. Spillane *et al.*, Phys. Rev. Lett. **98**, 122501 (2007).

[29] D. G. Yakovlev and D. A. Shalybkov, Sov. Sci. Rev. E. Astrophys. Space Phys. **7**, 311 (1989).

[30] A. Y. Potekhin and G. Chabrier, Astron. Astrophys. **538**, A115 (2012).

[31] L. R. Gasques, A. V. Afanasjev, M. Beard, J. Lubian, T. Neff, M. Wiescher, and D. G. Yakovlev, Phys. Rev. C **76**, 045802 (2007).

[32] A. Y. Potekhin, G. Chabrier, and F. J. Rogers, Phys. Rev. E **79**, 016411 (2009).

[33] A. Y. Potekhin, G. Chabrier, A. I. Chugunov, H. E. DeWitt, and F. J. Rogers, Phys. Rev. E **80**, 047401 (2009).

[34] A. I. Chugunov, Contrib. Plasma Phys. **52**, 114 (2012).

[35] S. Chandrasekhar, *Ellipsoidal Figures of Equilibrium* (Yale University Press, New Heaven, CT, 1969).

[36] B. Widom, J. Chem. Phys. **39**, 2808 (1963).